Title
El Niño-Driven Dry Season Flushing Enhances Dissolved Organic Matter Export From a Subtropical Watershed

Journal
Geophysical Research Letters, 47(19)

ISSN
0094-8276

Authors
Qu, Liyin
Wu, Yufang
Li, Yan
et al.

Publication Date
2020-10-16

DOI
10.1029/2020gl089877

Peer reviewed

Geophysical Research Letters

RESEARCH LETTER
10.1029/2020GL089877

El Niño-Driven Dry Season Flushing Enhances Dissolved Organic Matter Export From a Subtropical Watershed

Liyin Qu[1,2], Yufang Wu[3], Yan Li[4], Aron Stubbins[5], Randy A. Dahlgren[6], Nengwang Chen[1,2], and Weidong Guo[1,2]

[1]State Key Laboratory of Marine Environmental Science, College of Ocean and Earth Sciences, Xiamen University, Xiamen, China, [2]Fujian Provincial Key Laboratory for Coastal Ecology and Environmental Studies, Xiamen University, Xiamen, China, [3]Xiamen Environmental Monitoring Station, Xiamen, China, [4]Dongshan Swire Marine Station, Xiamen University, Xiamen, China, [5]Departments of Marine and Environmental Sciences, Civil and Environmental Engineering, and Chemistry and Chemical Biology, Northeastern University, Boston, MA, USA, [6]Department of Land, Air and Water Resources, University of California, Davis, CA, USA

These authors contributed equally to this work.

Key Points:

- 2015/2016 El Niño event induced a positive precipitation anomaly that increased $FDOM_H$ export during dry seasons from a subtropical watershed
- The wetter El Niño dry season was followed by lower $FDOM_H$ export during the subsequent wet season
- Watershed processes buffered $FDOM_H$ export relative to the El Niño-induced increase of precipitation/discharge

Supporting Information:

- Supporting Information S1

Correspondence to:
W. Guo,
wdguo@xmu.edu.cn

Citation:
Qu, L., Wu, Y., Li, Y., Stubbins, A., Dahlgren, R. A., Chen, N., & Guo, W. (2020). El Niño-driven dry season flushing enhances dissolved organic matter export from a subtropical watershed. *Geophysical Research Letters*, *47*, e2020GL089877. https://doi.org/10.1029/2020GL089877

Received 19 JUL 2020
Accepted 28 SEP 2020
Accepted article online 30 SEP 2020

Abstract The 2015/2016 super El Niño event resulted in a positive precipitation anomaly during dry seasons in the Jiulong River watershed, southeast China. Four years (2014–2017) of high frequency, in situ humic-like fluorescent DOM ($FDOM_H$) data in the Jiulong Estuary were coupled with extrapolation to a freshwater end-member $FDOM_H$ concentration and river discharge data to estimate riverine $FDOM_H$ export. The wetter El Niño dry season was followed by lower $FDOM_H$ export during the subsequent wet season. Furthermore, in the dry season after El Niño reached its strongest phase, a 90–187% increase in $FDOM_H$ export occurred. If widespread, this pattern suggests El Niño events may enhance export of $FDOM_H$ from south China rivers in dry seasons resulting in seasonal and annual shunting of the terrestrial DOM export, modulating coastal carbon cycling. This study highlights the need to incorporate climate-driven regulation patterns on DOM transport across the land-ocean interface.

1. Introduction

El Niño Southern Oscillation (ENSO) is one of the most significant climate perturbations on Earth. ENSO causes large-scale anomalous atmospheric circulation patterns and hydroclimate extremes (e.g., floods and droughts) around the world (Chen et al., 2017), dramatically changing terrestrial and oceanic carbon cycles (Bastos et al., 2018; Tian et al., 1998). The 2015/2016 super El Niño event, the strongest and longest-lasting event (i.e., 19 months) ever recorded, induced a widespread precipitation anomaly around the Pacific Ocean. Contrary to unprecedented high temperature and drought conditions in Southeast Asia and Australia (Pepler, 2016; Thirumalai et al., 2017), a strong positive precipitation anomaly occurred in southeast China and coastal areas of the temperate United States during the El Niño (Lim et al., 2017; Ma et al., 2018). In particular, a series of unusual rainstorm events occurred during the normal dry seasons, resulting in a seasonal to annual shift in hydrological patterns in affected watersheds.

Export of terrestrial dissolved organic matter (DOM) to coastal waters represents an important link between terrestrial and oceanic carbon pools (Battin et al., 2009; Bauer & Bianchi, 2011). Different from normal wet season rainstorm events (Fellman et al., 2009; Yang et al., 2013), the El Niño-driven "wet" dry season may induce a seasonal shunting of watershed DOM export and other perturbations (e.g., nutrients and suspended sediments) on coastal ecosystems. Due to their long-term duration, El Niño impacts exert much longer perturbations than episodic rainstorm events on riverine DOM export from watersheds (Medeiros et al., 2015). This implies that El Niño-regulated DOM export has a notable climate-driven regulation pattern on seasonal to annual time scales, unlike the weather-driven patterns occurring on much shorter time scales (Raymond et al., 2016). Due to lack of monitoring programs that cover entire El Niño life cycles, there is an important knowledge gap limiting our understanding of how these climate events regulate carbon cycle between the land-ocean interface.

Long-term perturbation of El Niño events on watersheds makes it crucial to deploy effective monitoring tools that provide reliable, continuous, and high-frequency DOM measurements, such as in situ optical fluorescent DOM (FDOM) sensors (Saraceno et al., 2009; Wymore et al., 2018). The excitation-emission wavelength of current commercial FDOM sensors represents humic-like FDOM ($FDOM_H$) components,

10.1029/2020GL089877

which are considered a good proxy for the terrestrial DOM fraction (Coble, 1996; Guo et al., 2014; Yang et al., 2019). In many aquatic systems, FDOM is highly correlated with DOC (Guo et al., 2011; Webb et al., 2018), suggesting that FDOM sensors provide an effective tool for monitoring watershed DOM dynamics and export (Shultz et al., 2018; Wymore et al., 2018).

Here we present 4 years (2014–2017) of $FDOM_H$ sensor data, demonstrating that the 2015/2016 El Niño-driven precipitation anomaly initiated an extraordinary dry season flushing of DOM from a subtropical river of southeast China. Confinement of this DOM flux within the winter monsoon-driven coastal currents suggests that the seasonal shunting of peak watershed DOM fluxes to coastal areas in El Niño years possibly changes CO_2 flux patterns between land-atmosphere and ocean-atmosphere interfaces. This study highlights the need to include spatiotemporal shunting of DOM export patterns by unusually "wet" dry seasons into models of DOM transport across the land-ocean interface.

2. Materials and Methods

2.1. Study Area

The Jiulong River, a medium-sized subtropical river in Fujian Province, China, has a length of 258 km and a drainage area of 14,741 km^2. Watershed land cover is dominated by forests (69.4%) (Yang et al., 2012). Mean population density is >200 persons per km^2, with intensive human activities (e.g., sewage discharge, agriculture, and animal husbandry) affecting water quality (Yu et al., 2015). Over 100 hydropower stations are distributed within the watershed, thus increasing the water residence time especially during the low flow period (Gao et al., 2018). The annual mean temperature and precipitation are 19.9–21.1°C and 1,400–1,800 mm, respectively. The hydrological cycle in Jiulong River watershed consists of a pre-dry season (January–March), wet season (April–September) that includes monsoon rain (April–June) and typhoon rain (July–September) periods, and post-dry season (October–December). The East Asian monsoon generally contributes ~75% of precipitation during the wet season (Huang, 2008). There are two major tributaries (north and west) to the Jiulong River that converge at the head of the Estuary, with a multi-year average runoff of 814 mm $year^{-1}$ discharging into the Taiwan Strait. Tides in the estuary are semidiurnal with a mean tidal range of 2.7–4.0 m (Guo et al., 2011).

2.2. Buoy Deployment and Data Processing

A buoy equipped with multi-parameter sensors (YSI, Yellow Springs, OH), including an EXO $FDOM_H$ Sensor Ti 599104-01 (Ex/Em = 365 ± 5/480 ± 40 nm) with automatic temperature compensation, was deployed at a depth of 0.8 m in the middle reach of Jiulong River Estuary (Figure S1a in the supporting information). This location avoided the estuarine turbidity maximum zone in the upper estuary. A central wiper and copper tape were installed on the sonde to inhibit biofouling. All sensor data (temperature, salinity, turbidity, and $FDOM_H$) were collected at a 30 min interval. Fluorescence intensity of the $FDOM_H$ sensor was standardized to quinine sulfate units (QSUs) using a two-point calibration during monthly maintenance.

As an optical monitoring tool, the FDOM sensor performance was susceptible to inner filter effects (IFEs) caused by high DOC and turbidity concentrations (Downing et al., 2012). As a result, correction procedures are often necessary for obtaining reliable data (see details in the supporting information). After correction, 92.7% of $FDOM_H$ data were available for analysis during the study period (1 January 2014 to 31 December 2017). We were not able to correct 1.6% of the data due to high turbidity during the flood tide period and equipment malfunction or maintenance accounted for the remaining 5.7% of the missing data record.

2.3. Estimate of River End-Member $FDOM_H$ and Flux Calculation

$FDOM_H$ for the river end-member was estimated using the classical effective concentration method (Officer, 1979; Figures S2a–S2c). As all $FDOM_H$ data within each tide cycle showed strong conservative mixing behavior in medium and high salinity waters (R^2: 0.95 ± 0.06) (Figure S3), a simple regression line was established for each flood/ebb tide and extrapolated to zero salinity to obtain the effective $FDOM_H$ (C_0, QSU). The actual river end-member $FDOM_H$ was lower than this effective $FDOM_H$ due to contributions from estuarine addition (e.g., particle desorption and sediment resuspension) in low-salinity waters (Guo et al., 2011). However, effective $FDOM_H$ reflects the variation tendency of the river end-member $FDOM_H$ as the seasonal bias from estuarine addition was small (~2%), with slightly higher additions only during the drought season (~5%). This small bias did not influence the statistical significance of $FDOM_H$ between different seasons (see sections 4.2 and 4.3). Daily $FDOM_H$ was the average of estimated $FDOM_H$ for each tide cycle. For missing/uncorrectable sensor data that occurred at steady-flow conditions, the daily $FDOM_H$ of the river end-member was estimated by a mathematical smoothing method. For missing/uncorrectable sensor data that occurred during storm event periods, missing peak values were set as two times that of the smoothed data based on a previous storm event study (Yang et al., 2013).

The daily $FDOM_H$ flux was determined as

$$F_{\mathrm{FDOM}} = C_{0\mathrm{d}} \times Q_{\mathrm{d}}, \tag{1}$$

where F_{FDOM} represents the export $FDOM_H$ flux eventually discharged into the sea (Officer, 1979), which included a relatively stable estuarine addition flux throughout the different seasons (Guo et al., 2011), and $C_{0\mathrm{d}}$ and Q_{d} are daily effective $FDOM_H$ (QSU) and daily discharge (m^3 day^{-1}, from hydrological stations on North and West River tributaries; Figure S1a). As one QSU is equal to the fluorescence intensity of 1 μg L^{-1} (i.e., 10^3 μg QS equivalent m^{-3}) quinine sulfate (QS) at 350 nm excitation and 450 nm emission wavelengths, the units of daily $FDOM_H$ flux were μg QS equiv day^{-1} (Yamashita & Tanoue, 2008).

To identify the $FDOM_H$ flux contributed by rainstorm events, baseflow was first calculated by an automatic segmentation procedure (Smoothed Minima method) (Nathan & Mcmahon, 1990). A storm event was designated as a flow peak that exceeded two times the yearly average discharge, and which started and ended when discharge was more than 1.2 times the previous baseflow (Gao et al., 2018). The antecedent precipitation index (*API*) was calculated as

$$API = \sum K^i P_i, \tag{2}$$

where K is a constant ($K = 0.85$) and P_i is precipitation for 1, 2, 3, ..., i days ($i = 14$) prior to the flood event (API < 15: dry; 15 < API < 30: medium; API > 30: wet).

3. Results

The hydrological cycle in Jiulong River watershed showed large annual and seasonal variations between 2014 and 2017. Total annual precipitation was 1,518, 1,754, 2,314, and 1,350 mm (Figure 1b), with significantly ($p < 0.05$) higher precipitation in the 2016 El Niño year. The number of rainstorm events (11) in 2016 was also higher than the other years (6, 9, and 6 for 2014, 2015, and 2017; Table S1). At the seasonal scale, precipitation during the wet season across all 4 years showed no significant difference ($p > 0.05$; Figure 1c). However, precipitation amounts for both pre-dry and post-dry seasons of 2016 (604 and 408 mm) and post-dry season of 2015 (235 mm) were all significantly higher than other dry seasons (73–199 mm; $p < 0.05$). Notably, abnormal rainfall events in the pre-dry season of 2016 (Figure 1c) delivered as much precipitation as its wet season, creating a large anomaly to the normal precipitation pattern.

Daily discharge of the Jiulong River from 2014 to 2017 fluctuated between 0.4 and 27.0 mm day^{-1}, with average annual discharge of 2.1, 2.3, 4.3, and 2.3 mm day^{-1}, respectively (Figure 1b). Consistent with the higher precipitation and frequent rainstorm events in 2016 (Table S1), discharge in 2016 was also higher than the other 3 years ($p < 0.05$). At the seasonal scale, discharge in both wet and dry seasons of 2016 was higher than the respective wet and dry seasons of the other 3 years ($p < 0.05$; Figure 1d). Notably, discharge in the two dry seasons of 2016 showed no difference from the other wet seasons ($p > 0.05$; Figure 1d). The atypical six storm events during the 2016 dry seasons had high average (3.6–7.6 mm day^{-1}) and peak (9.5–24.8 mm day^{-1}) discharges. In contrast, storm events in dry seasons of the other years were only observed in late 2015 and early 2017 and had much lower average (2.5–3.8 mm day^{-1}) and peak (5.2–10.1 mm day^{-1}) discharges.

Daily $FDOM_H$ of the freshwater end-member ranged from 5.2 to 45.3 QSU (Figure 1b), with an average of 19.7 ± 5.4 QSU from 2014 to 2017. Annual average $FDOM_H$ in 2016 (14.7 ± 4.7 QSU) was lower than the other 3 years (2014: 21.4 ± 3.6; 2015: 21.5 ± 5.4; and 2017: 21.2 ± 4.7 QSU) ($p < 0.05$). At the seasonal scale, $FDOM_H$ in the dry seasons of 2014/2015 and post-dry season of 2017 was significantly higher ($p < 0.05$) than the other dry seasons (Figure 1e). $FDOM_H$ consistently decreased from the 2015 pre-dry season to their lowest average values in the 2016 pre-dry season, followed by a general increase through 2017. At the

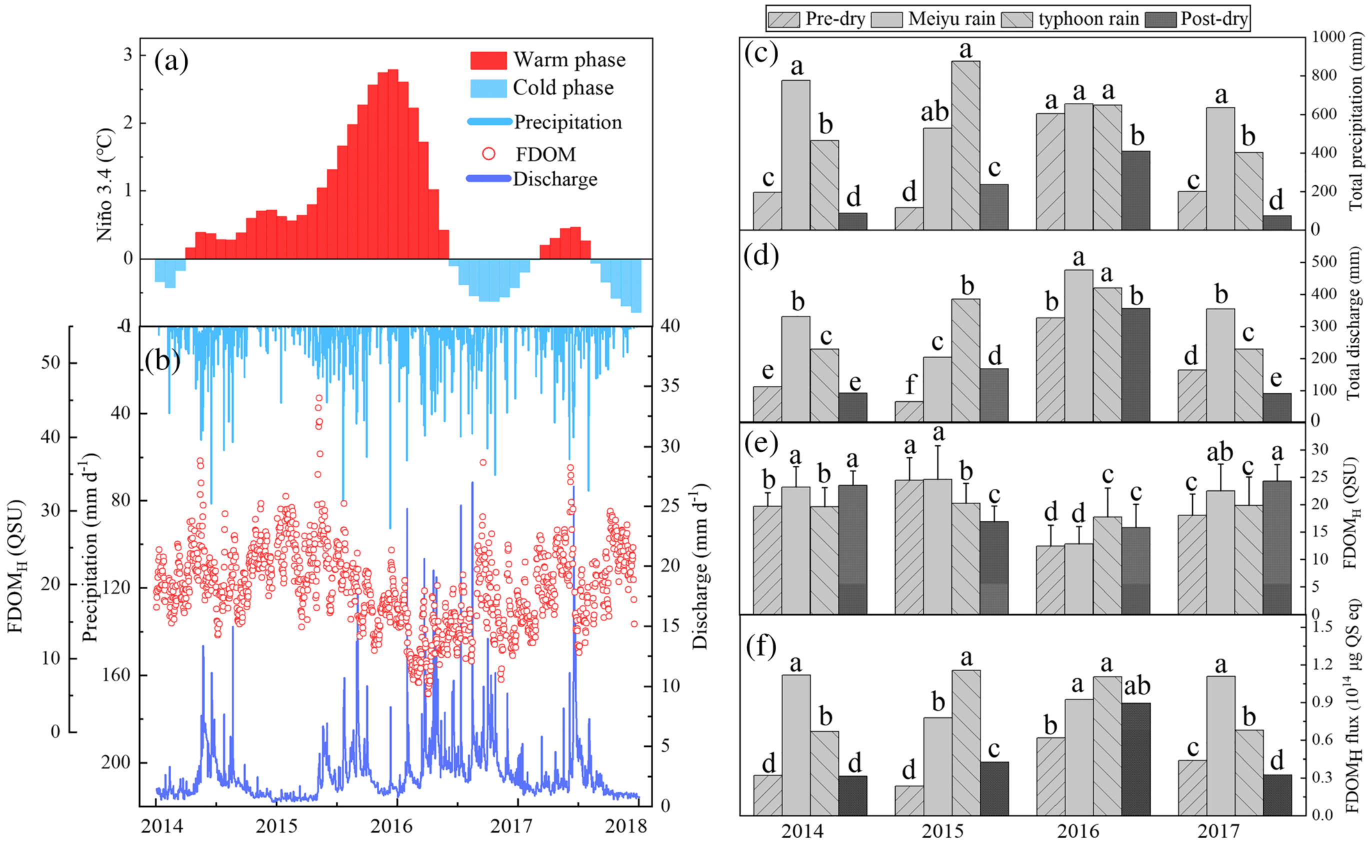

Figure 1. El Niño 3.4 index, meteorological, hydrological, and freshwater (river) end-member $FDOM_H$ data in Jiulong River watershed during the study period. (a) Niño 3.4 index is a 3-month running mean of sea surface temperature anomalies; (b) time series of daily precipitation, river discharge, and freshwater end-member $FDOM_H$. Daily precipitation data were the average of eight weather stations distributed throughout the watershed (http://www.weather.com.cn/). (c–f) Seasonal variation of total precipitation, total discharge, daily average $FDOM_H$, and total $FDOM_H$ flux in the four hydrologic seasons. Different letters indicate significant difference at $p < 0.05$.

storm-event scale, $FDOM_H$ showed two contrasting responses to discharge fluctuations. (Type I) peak $FDOM_H$ occurred before or was coincident with peak discharge (Figures 2 and S4), while (Type II) peak $FDOM_H$ occurred later than peak discharge (Figures 2 and S5). Notably, the antecedent precipitation index (*API*) of Type I events (16.9 ± 9.0 mm), an assessment of catchment moisture status prior to a storm event (Table S1), was significantly lower than for Type II events (20.5 ± 14.1 mm) ($p < 0.05$).

Annual $FDOM_H$ export fluxes from the Jiulong River watershed were 2.42×10^{14}, 2.59×10^{14}, 3.54×10^{14}, and 2.64×10^{14} μg QS equiv year^{-1} from 2014 to 2017, respectively (Table S2). The $FDOM_H$ flux in 2016 was 136–146% higher than the other 3 years ($p < 0.05$). The percentage contribution of $FDOM_H$ fluxes by storm events accounted for as high as 69% in 2016 (Table S2). At the seasonal scale, $FDOM_H$ fluxes in wet seasons were higher than dry seasons ($p < 0.05$; Figure 1f). Further, fluxes in the 2016 dry seasons were higher than in other dry seasons ($p < 0.05$; Figure 1f). The percentage of flux contributions by storm events during dry seasons from late 2015 to early 2017 were 45%, 75%, 70%, and 24%, respectively (Table S2). $FDOM_H$ fluxes in other dry seasons were contributed only by baseflow.

4. Discussion

4.1. Hydrologic Response to 2015/2016 El Niño Event

The 2015/2016 super El Niño event created abnormal precipitation events across many global regions (e.g., Southeast China and Western United States) (Chen et al., 2018; Lim et al., 2018; Ma et al., 2018). In the Jiulong River watershed, a total of 10 rainfall events occurred during the dry seasons from late 2015 to early 2017 (Table S1). In particular, extremely high precipitation occurred during the pre-dry season of 2016 after the peak of this extreme climatic event (December 2015). High precipitation also occurred

10.1029/2020GL089877

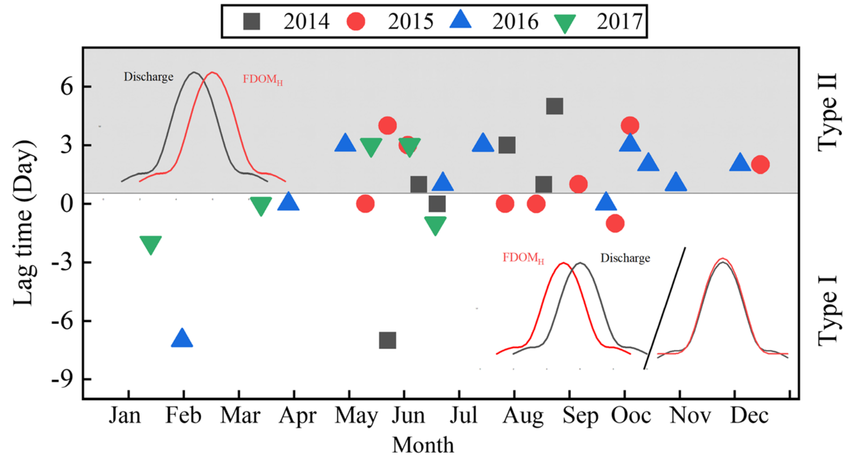

Figure 2. Assessment of two types of storm events for the study period (2014–2017) based on the lag time between peak $FDOM_H$ and peak discharge (after correction for the time difference between peak discharge and minimum sensor salinity within each storm event). Negative or zero lag times indicate peak $FDOM_H$ occurs before or is coincident with peak discharge (Type I). Positive lag time implies peak $FDOM_H$ occurs later than peak discharge (Type II). The lag times of all events were evaluated by linear regression tests.

during the post-dry season of 2016 after the positive sea surface temperature anomalies over the basin-wide Indian Ocean in summer of 2016 (Chen et al., 2018). This indicates a 1–2 month lag time in the precipitation response to the 2015/2016 El Niño event ($p < 0.05$; Figure S6).

Delay in the regional climate response to super El Niño events was previously reported (Ma et al., 2018). El Niño events may cause a large-scale anomaly for the western North Pacific anticyclone (WNPAC) (Yuan & Yang, 2012). The WNPAC enhances precipitation in southeastern China through modulating the western North Pacific subtropical high and further regulating atmospheric moisture transport (Chen et al., 2014). Given the time required for atmospheric moisture transport, the precipitation lag period in Jiulong River watershed maybe expected. Indeed, El Niño-related WNPAC could persist from an El Niño winter to the subsequent summer, even if the El Niño has already dissipated (Chen et al., 2018). Thus, we posit that the above-normal rainfall anomaly in dry seasons from late 2015 to early 2017 was directly related to the 2015/2016 El Niño event (Figure 1c).

Discharge patterns of Jiulong River generally followed the variation of precipitation in the watershed (Figures 1c and 1d), consistent with the general regulation mode of river runoff by watershed rainfall (Gao et al., 2018; Yang et al., 2013). Although the precipitation amount in the 2016 pre-dry and wet seasons showed no difference ($p > 0.05$), the runoff in the wet season was significantly higher than the pre-dry season ($p < 0.05$) (Figure 1d). Soil moisture status in the watershed increased after the El Niño-induced increase of rainfall during the 2015/2016 dry seasons. As a result, the runoff-to-rainfall coefficient in the 2016 wet season increased; that is, a greater fraction of rainfall becomes runoff as opposed to recharging soil water storage (Norbiato et al., 2009). Likewise, the rainfall amount in the 2016 post-dry season was lower than in the pre-dry season ($p < 0.05$), but the post-dry season runoff maintained a similar level ($p > 0.05$) (Figures 1c and 1d).

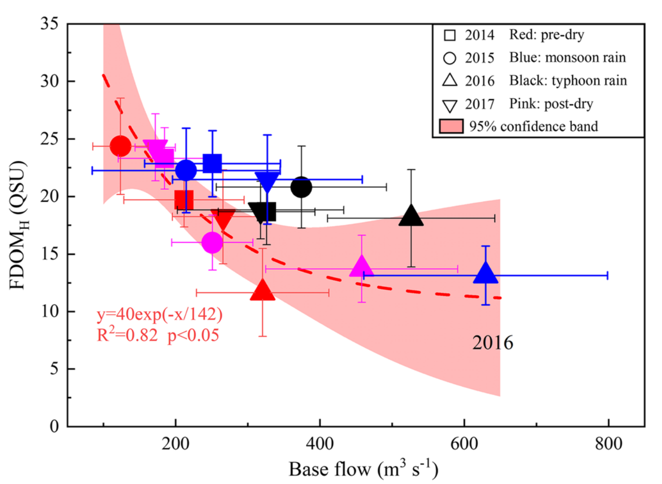

Figure 3. Relationship of $FDOM_H$ concentration and baseflow discharge (mean ± std dev). Baseflow is defined as the time between storm events.

4.2. Response of $FDOM_H$ Dynamics and Fluxes to El Niño Event During Dry Seasons

Consistent with the distinct changes in dry season hydrology, $FDOM_H$ dynamics during baseflow periods of dry seasons also changed. The highest $FDOM_H$ concentrations (24 ± 3.3 QSU) occurred in the non-El Niño 2014/2015 dry seasons and 2017 post-dry season, that is, the lowest baseflow periods during the 2014–2017 study (Figure 3). These $FDOM_H$ values remained the highest and were higher than other seasons ($p < 0.05$) even after subtracting the additional signal (~5%) from low-salinity estuary waters during drought seasons (Guo et al., 2011). Similarly high $FDOM_H$ followed an extreme drought period during the 2008/2009 dry seasons in this watershed (Guo et al., 2011; Hong et al., 2012). During drought periods, the reduction of river flow, exacerbated by reservoir impoundment, increased water residence time and enhanced in situ production of $FDOM_H$ in this eutrophic river (Hong et al., 2012). $FDOM_H$ derived from agricultural and urban pollution sources also accumulates in the fluvial system during drought periods (Wilson & Xenopoulos, 2009). Although multiple sources contributed to increased $FDOM_H$ concentration, total $FDOM_H$ export flux reached its lowest levels due to the large reduction of discharge (Table S2).

As baseflow discharge during dry seasons increased, $FDOM_H$ decreased (Figure 3, $p < 0.05$) and reached its lowest values in the 2016 pre-dry season (11.6 QSU ± 2%). This indicates that a dilution effect regulates $FDOM_H$ dynamics under El Niño-induced high baseflow conditions. Similar to other storm-event studies in many global watersheds (Fellman et al., 2009; Yang et al., 2013), two extraordinary Type I storm events flushed large amounts of $FDOM_H$ from the watershed (Figure 2). Low antecedent soil moisture (API index: 3.7 and 21.8 mm) and the occurrence of the $FDOM_H$ peak earlier than peak discharge (Figure S4) indicate that $FDOM_H$ was flushed mainly from readily mobilized pools stored in the watershed through surficial flow paths during the early phase of the event (Mann et al., 2012). The $FDOM_H$ source in surficial flow paths could originate from litter leaching and/or anthropogenic sources (Yang et al., 2012). Rapid decrease of $FDOM_H$ during and after peak discharge suggest that the contribution from soil interflow (i.e., leachable $FDOM_H$ in the soil profile) was small during Type I storm events (Yang et al., 2013). Following this flushing process, $FDOM_H$ in baseflow was diluted as further DOM contributions were limited (Bao et al., 2019). As a result, although $FDOM_H$ flux in this "wetter" dry season was 93% and 161% higher than in the normal pre-dry seasons of 2014 and 2015, its increased magnitude was only 40–48% of the corresponding increase in discharge (192% and 400%, respectively). This demonstrates a dilution-induced buffering effect for watershed DOM export under perturbation by the El Niño-induced precipitation anomaly. This is clearly illustrated by the lower rate of increase for cumulative $FDOM_H$ flux compared with cumulative discharge flux (Figure S7) (i.e., deviation below the 1:1 line) after storm events in January 2016. There was a similar, but much weaker, tendency in early 2017 when the El Niño event had nearly dissipated (Figure S7).

The cumulative discharge flux for the 2016 post-dry season was as high as the pre-dry season of 2016, but its $FDOM_H$ export flux was significantly higher than the latter ($p < 0.05$). This suggests a different $FDOM_H$ regulating mechanism for this "wetter" dry season. Precipitation before this post-dry season (1,906 mm) was even higher than the annual precipitation in normal years (1,400–1,800 mm). The high antecedent soil moisture (Table S1) suggests strong $FDOM_H$ leaching from the soil profile via increased contributions from soil interflow (Bao et al., 2019; Yang et al., 2013). As this hydrologic flow path has an appreciable lag time relative to surficial runoff, there is a delay in the $FDOM_H$ peak relative to the discharge peak for three Type II storm events (Figure S5). The increased contribution of soil-derived humic DOM resulted in the baseflow $FDOM_H$ in this pos-dry season being higher than in the pre-dry season ($p < 0.05$) (Figures 1e and 3). High soil moisture status also made the baseflow of the 2016 post-dry season significantly higher than the pre-dry season ($p < 0.05$). As a result, the flux contributed by baseflow in this season was significantly increased. Together with the contribution by storm events (Table S2), $FDOM_H$ flux in the 2016 post-dry season was the highest among all dry seasons (Figure 1f).

4.3. Coupling $FDOM_H$ Dynamics in Monsoon Season With Hydrology of Preceding Dry Season

In monsoon seasons (early stage of wet season), variations in $FDOM_H$ levels and flux showed contrasting patterns between normal and El Niño years. The average $FDOM_H$ in 2015 was clearly above the $FDOM_H$-baseflow curve of the dry season (Figure 3). The rate of increase in $FDOM_H$ flux was higher than the rate of increase for the discharge flux in 2015 (Figure S7). However, average $FDOM_H$ in the 2016 El Niño year was among the lowest of all monsoon periods and close to the dry season curve (Figure 3). As a result, the rate of increase in $FDOM_H$ flux was lower than the rate of increase for the discharge flux in 2016 (Figure S7).

There were large differences between the API index and the first storm-event type during the monsoon seasons of El Niño and non-El Niño years (Table S1 and Figure 2). This suggests that the hydrologic conditions associated with the pre-dry season may closely regulate $FDOM_H$ dynamics of the subsequent monsoon season. The low API index (16.7 mm) of a Type I storm event (Event 7) in the 2015 monsoon period suggests that there was effective flushing of $FDOM_H$ stored in the watershed during the extreme dry season drought of 2015. A similar "first-flush effect" for nitrogen and phosphorus has been observed in the Jiulong River watershed and other watersheds (Chen et al., 2015; Ribarova et al., 2008). A dominance of surficial flow paths and the beginning of agricultural activities during this period could provide major sources of $FDOM_H$ (Eckard et al., 2017). In contrast, the variation of $FDOM_H$ and discharge flux rates in 2016 indicates a watershed buffering effect for DOM due to dilution that continued to dominate $FDOM_H$ dynamics after the El Niño-induced "wetter" pre-dry season. Thus, $FDOM_H$ dynamics in the Jiulong River watershed during monsoon seasons demonstrate a close coupling with the hydrology of the preceding dry seasons: enhanced flushing pattern in normal hydrological years versus a buffering effect pattern in El Niño years (Figure 3).

4.4. Significance of El Niño Events on Carbon Cycle Between Land and Ocean

The 2015/2016 super El Niño event triggered a seasonal shunting of $FDOM_H$ export from the Jiulong River watershed. The general pattern of $FDOM_H$ storage in dry seasons followed by wet season flushing in normal hydrological years (i.e., 2014 and 2015) was replaced by an advanced flushing by dry season storm events in the El Niño year. This resulted in a pulse of $FDOM_H$ export in the pre-dry season of 2016. $FDOM_H$ export fluxes were 90–187% higher than that of the 2014 and 2015 pre-dry seasons after El Niño reached its strongest phase. Similar to other river and estuarine systems (Bauer & Bianchi, 2011; Saraceno et al., 2009; Wymore et al., 2018), there was a significant correlation between $FDOM_H$ and DOC in the Jiulong River Estuary (Figure S8; Guo et al., 2011). Thus, it is expected that the export pattern of DOC from Jiulong River resembles that of $FDOM_H$.

On the larger regional scale, a significant increase of discharge during the El Niño dry period was widespread throughout rivers of south and central China (Table S3). For the two largest rivers in China, the Yangtze and Pearl Rivers (Lin, 2007), which have an average discharge 69 and 28 times higher than the Jiulong River (Milliman & Farnsworth, 2011), discharge during the dry seasons of the El Niño year (2016) was 41–55% and 206–247% higher than in 2014 and 2015. The increase in discharge was much higher for medium and smaller rivers (26–864%), with an average increase of 238% (Table S3). For illustration purposes, we assumed that the watershed buffering effect for these medium and smaller rivers was similar to the Jiulong River (i.e., increase of DOM flux was ~40% of discharge increase) and the large Yangtze and Pearl Rivers had no appreciable buffering effect (Bao et al., 2015). Based on this assumption, the El Niño-induced increase of DOM export to Chinese coastal waters during the post-dry season of 2015 and pre-dry season of 2016 would reach 23–30% and 82–93% higher than the same periods of non-El Niño years, respectively.

Driven by the dominant northeast winter Asian monsoon in dry seasons, El Niño-flushed terrestrial DOM is transported southward along the coasts by the Chinese Coastal Current (Figure S1b). $FDOM_H$ (determined at 365/460 nm) usually represents relatively biologically recalcitrant dissolved organic matter (RDOM) in fluvial systems, and photobleaching/photodegradation destruction of RDOM in the winter dry season is lower than the summer wet season. Thus, the El Niño-enhanced fluvial DOM fluxes may be transported greater distances, thereby enhancing marine carbon cycling and processing as far south as the coast of Viet Nam (Zheng et al., 2006). In contrast, large storm events during wet seasons can often inject a portion of the DOM flux into the open ocean. Given that much of the terrestrial-derived DOM will be eventually degraded to CO_2 (Bianchi et al., 2013; Osburn et al., 2019), El Niño-enhanced transfer of terrestrially derived carbon to the ocean can result in losses of stored carbon from soils to the atmosphere, thereby having a strong impact on coastal carbon cycling dynamics.

On the global scale, it can be expected that the 2015/2016 super El Niño event would similarly enhance DOM export from land to ocean in the western and eastern United States due to increased rainfall and subsequent runoff/leaching (Lim et al., 2018; Yoon & Raymond, 2012). In contrast, a decrease of DOM fluxes may have occurred in parts of southeast Asia (Thirumalai et al., 2017) and the Amazon basin (Bastos et al., 2018) due to extreme drought events. Thus, the 2015/2016 El Niño event could contribute to latitudinal adjustments in terrestrial DOM export. As extreme El Niño events are projected to occur more frequently in a warming world (Thirumalai et al., 2017) and extreme events are not predictable, deployment of long-term FDOM and water quality monitoring programs is necessary across several global river and estuarine systems to provide critical information to improve assessments of DOM dynamics in response to climatic perturbations (Carstea et al., 2020).

5. Conclusions

Results from our 4-year, high-frequency $FDOM_H$ sensor revealed that a super El Niño event induced seasonal shunting of DOM transport between the land-sea interface. As the dry seasons became much wetter in response to the extreme 2015/2016 El Niño event, there was extraordinary dry season DOM flushing from our watershed in south-central China, influencing carbon biogeochemistry of widespread coastal ecosystems. The wetter El Niño dry season was followed by lower $FDOM_H$ export during the subsequent wet season. These results highlight the need to include annual and seasonal scale DOM export dynamics, as regulated by ENSO events, into models of DOM transport across the land-ocean interface. In situ protein-like fluorescence sensors, which represent biologically labile DOM components, should also be considered in addition to $FDOM_H$ sensors, to provide a powerful tool to assess short-term (e.g., storm events), medium-term (e.g., El Niño or drought events), and long-term perturbations (e.g., climate change) to DOM biogeochemistry in terrestrial and marine ecosystems.

Conflicts of Interest

The authors declared that they have no conflicts of interest to this work.

Data Availability Statement

Daily precipitation and $FDOM_H$ data are available at 4TU.Research Data (http://doi.org/10.4121/uuid:1b233566-0330-4a23-aade-0b61c3460881).

Acknowledgments
This work was jointly supported by grants from the National Natural Science Foundation of China (U1805241, 41876083, and 41676098) and Fundamental Research Funds for the Universities of China (20720180119 and 20720190105). We thank Mr. Dapeng Huang from Xiamen Hanhong Environment Technology Company for his valuable technical support in maintaining the long-term buoy/sonde sensors. We especially thank Prof. Jinliang Huang, Prof. Weidong Zhai, and faculty/staff from the MEL Ocean Data Center of Xiamen University for sharing river discharge data (http://xxfb.mwr.cn/sq_djdh.html). We thank Jing Xu for data processing and Dr. Yuwu Jiang for his valuable comments. We would like to thank Dr. Jamie Shanley and another anonymous reviewer for their valuable comments and suggestions to improve our manuscript.

References

Bao, H., Niggemann, J., Huang, D., Dittmar, T., & Kao, S. (2019). Different responses of dissolved black carbon and dissolved lignin to seasonal hydrological changes and an extreme rain event. *Journal of Geophysical Research: Biogeosciences*, *124*, 479–493. https://doi.org/10.1029/2018JG004822

Bao, H., Wu, Y., & Zhang, J. (2015). Spatial and temporal variation of dissolved organic matter in the Changjiang: Fluvial transport and flux estimation. *Journal of Geophysical Research: Biogeosciences*, *120*, 1870–1886. https://doi.org/10.1002/2015JG002948

Bastos, A., Friedlingstein, P., Sitch, S., Chen, C., Mialon, A., Wigneron, J. P., et al. (2018). Impact of the 2015/2016 El Niño on the terrestrial carbon cycle constrained by bottom-up and top-down approaches. *Philosophical Transactions of the Royal Society B*, *373*(1760), 20170304. https://doi.org/10.1098/rstb.2017.0304

Battin, T. J., Luyssaert, S., Kaplan, L. A., Aufdenkampe, A. K., Richter, A., & Tranvik, L. J. (2009). The boundless carbon cycle. *Nature Geoscience*, *2*(9), 598–600. https://doi.org/10.1038/ngeo618

Bauer, J. E., & Bianchi, T. S. (2011). Dissolved organic carbon cycling and transformation. In E. Wolanski & D. S. McLusky (Eds.), *Treatise on estuarine and coastal science* (Vol. 5, pp. 7–67). Waltham: Academic Press. https://doi.org/10.1016/B978-0-12-374711-2.00502-7

Bianchi, T. S., Garcia-Tigreros, F., Yvon-Lewis, S. A., Shields, M., Mills, H. J., Butman, D., et al. (2013). Enhanced transfer of terrestrially derived carbon to the atmosphere in a flooding event. *Geophysical Research Letters*, *40*, 116–122. https://doi.org/10.1029/2012GL054145

Carstea, E. M., Popa, C. L., Baker, A., & Bridgeman, J. (2020). In situ fluorescence measurements of dissolved organic matter: A review. *Science of the Total Environment*, *699*, 134361. https://doi.org/10.1016/j.scitotenv.2019.134361

Chen, J., Wen, Z., Wu, R., Chen, Z., & Zhao, P. (2014). Interdecadal changes in the relationship between Southern China winter-spring precipitation and ENSO. *Climate Dynamics*, *43*(5–6), 1327–1338. https://doi.org/10.1007/s00382-013-1947-x

Chen, J., Wang, X., Zhou, W., Wang, C., Xie, Q., & Li, G. (2018). Unusual rainfall in southern China in decaying August during extreme EI Niño 2015/16: Role of the western Indian Ocean and north tropical Atlantic SST. *Journal of Climate*, *31*(17), 7019–7034. https://doi.org/10.1175/JCLI-D-17-0827.1

Chen, L., Li, T., Wang, B., & Wang, L. (2017). Formation mechanism for 2015/16 Super El Niño. *Scientific Reports*, *7*(1), 2975–2984. https://doi.org/10.1038/s41598-017-02926-3

Chen, N., Wu, Y., Chen, Z., & Hong, H. (2015). Phosphorus export during storm events from a human perturbed watershed, southeast China: Implications for coastal ecology. *Estuarine, Coastal and Shelf Science*, *166*(2015), 178–188. https://doi.org/10.1016/j.ecss.2015.03.023

Coble, P. G. (1996). Characterization of marine and terrestrial DOM in seawater using excitation-emission matrix spectroscopy. *Marine Chemistry*, *51*(4), 325–346. https://doi.org/10.1016/0304-4203(95)00062-3

Downing, B. D., Pellerin, B. A., Bergamaschi, B. A., Saraceno, J. F., & Kraus, T. E. C. (2012). Seeing the light: The effects of particles, dissolved materials, and temperature on in situ measurements of DOM fluorescence in rivers and streams. *Limnology and Oceanography: Methods*, *10*(10), 767–775.

Eckard, R. S., Pellerin, B. A., Bergamaschi, B. A., Bachand, P. A., Bachand, S. M., Spencer, R. G., & Hernes, P. J. (2017). Dissolved organic matter compositional change and biolability during two storm runoff events in a small agricultural watershed. *Journal of Geophysical Research: Biogeosciences*, *122*, 2634–2650. https://doi.org/10.1002/2017JG003935

Fellman, J. B., Hood, E., Edwards, R. T., & Damore, D. V. (2009). Changes in the concentration, biodegradability, and fluorescent properties of dissolved organic matter during stormflows in-coastal temperate watersheds. *Journal of Geophysical Research*, *114*, G01021. https://doi.org/10.1029/2008JG000790

Gao, X., Chen, N., Yu, D., Wu, Y., & Huang, B. (2018). Hydrological controls on nitrogen (ammonium versus nitrate) fluxes from river to coast in a subtropical region: Observation and modeling. *Journal of Environmental Management*, *213*, 382–391. https://doi.org/10.1016/j.jenvman.2018.02.051

Guo, W., Yang, L., Hong, H., Stedmon, C. A., Wang, F., Xu, J., & Xie, Y. (2011). Assessing the dynamics of chromophoric dissolved organic matter in a subtropical estuary using parallel factor analysis. *Marine Chemistry*, *124*(1–4), 125–133. https://doi.org/10.1016/j.marchem.2011.01.003

Guo, W., Yang, L., Zhai, W., Chen, W., Osburn, C., Huang, X., & Li, Y. (2014). Runoff-mediated seasonal oscillation in the dynamics of dissolved organic matter in different branches of a large bifurcated estuary: The Changjiang Estuary. *Journal of Geophysical Research: Biogeosciences*, *119*, 776–793. https://doi.org/10.1002/2013JG002540

Hong, H., Yang, L., Guo, W., Wang, F., & Yu, X. (2012). Characterization of dissolved organic matter under contrasting hydrologic regimes in a subtropical watershed using PARAFAC model. *Biogeochemistry*, *109*(1-3), 163–174. https://doi.org/10.1007/s10533-011-9617-8

Huang, X. Q. (2008). Hydrologic characteristics of Jiulong River watershed. *Hydraulic Science and Technology*, *01*, 16–20. (In Chinese)

Lim, Y. K., Kovach, R. M., Pawson, S., & Vernieres, G. (2017). The 2015/16 El Niño event in context of the MERRA-2 reanalysis: A comparison of the tropical Pacific with 1982/83 and 1997/98. *Journal of Climate*, *30*(13), 4819–4842. https://doi.org/10.1175/JCLI-D-16-0800.1

Lim, Y. K., Schubert, S. D., Chang, Y., Molod, A., & Pawson, S. (2018). The impact of SST-forced and unforced teleconnections on 2015/16 El Niño winter precipitation over the western United States. *Journal of Climate*, *31*(15), 5825–5844. https://doi.org/10.1175/JCLI-D-17-0218.1

Lin, J. (2007). On the behavior and fluxes of dissolved organic carbon in two large Chinese estuaries—Changjiang and Zhujiang (Master's thesis). Xiamen: Xiamen University. Retrieved from https://etd.xmu.edu.cn/default.asp

Ma, F., Ye, A., You, J., & Duan, Q. (2018). 2015–16 floods and droughts in China, and its response to the strong El Niño. *Science of the Total Environment*, *627*, 1473–1484. https://doi.org/10.1016/j.scitotenv.2018.01.280

Mann, P. J., Davydova, A., Zimov, N., Spencer, R. G. M., Davydov, S., Bulygina, E., et al. (2012). Controls on the composition and lability of dissolved organic matter in Siberia's Kolyma River basin. *Journal of Geophysical Research*, *117*, G01028. https://doi.org/10.1029/2011JG001798

Medeiros, P. M., Seidel, M., Dittmar, T., Whitman, W. B., & Moran, M. A. (2015). Drought-induced variability in dissolved organic matter composition in a marsh dominated estuary. *Geophysical Research Letters*, *42*, 6446–6453. https://doi.org/10.1002/2015GL064653

Milliman, J. D., & Farnsworth, K. L. (2011). *River discharge to the coastal ocean: A global synthesis* (pp. 288–311). Cambridge: Cambridge University Press. https://doi.org/10.1017/CBO9780511781247

Nathan, R. J., & Mcmahon, T. A. (1990). Evaluation of automated techniques for base flow and recession analyses. *Water Resources Research*, *26*(7), 1465–1473. https://doi.org/10.1029/WR026i007p01465

Norbiato, D., Borga, M., Merz, R., Blőschl, G., & Carton, A. (2009). Controls on event runoff coefficients in the eastern Italian Alps. *Journal of Hydrology*, *375*(3–4), 312–325. https://doi.org/10.1016/j.jhydrol.2009.06.044

Officer, C. B. (1979). Discussion of the behaviour of the non-conservative dissolved constituents in estuaries. *Estuarine and Coastal Marine Science*, *9*, 911–994.

Osburn, C. L., Rudolph, J. C., Paerl, H. W., Hounshell, A. G., & van Dam, B. R. (2019). Lingering carbon cycle effects of Hurricane Matthew in North Carolina's coastal waters. *Geophysical Research Letters*, *46*, 2654–2661. https://doi.org/10.1029/2019GL082014

Pepler, A. S. (2016). Seasonal climate summary southern hemisphere (summer 2015–16): Strong El Niño peaks and begins to weaken. *Journal of Southern Hemisphere Earth Systems Science*, *66*, 361–379.

Raymond, P. A., Saiers, J. E., & Sobczak, W. V. (2016). Hydrological and biogeochemical controls on watershed dissolved organic matter transport: Pulse-shunt concept. *Ecology*, *97*(1), 5–16. https://doi.org/10.1890/14-1684.1

Ribarova, I., Ninov, P., & Cooper, D. (2008). Modeling nutrient pollution during a first flood event using HSPF software: Iskar River case study, Bulgaria. *Ecological Modelling*, *211*(1–2), 241–246. https://doi.org/10.1016/j.ecolmodel.2007.09.022

Saraceno, J. F., Pellerin, B. A., Downing, B. D., Boss, E., Bachand, P. A. M., & Bergamaschi, B. A. (2009). High-frequency in situ optical measurements during a storm event: Assessing relationships between dissolved organic matter, sediment concentrations, and hydrologic processes. *Journal of Geophysical Research: Biogeosciences*, *114*.

Shultz, M., Pellerin, B. A., Aiken, G. R., Martin, J., & Raymond, P. A. (2018). High frequency data exposes nonlinear seasonal controls on dissolved organic matter in a large watershed. *Environmental Science & Technology*, *52*(10), 5644–5652. https://doi.org/10.1021/acs.est.7b04579

Thirumalai, K., Dinezio, P. N., Okumura, Y., & Deser, C. (2017). Extreme temperatures in Southeast Asia caused by El Niño and worsened by global warming. *Nature Communications*, *8*(1), 15531. https://doi.org/10.1038/ncomms15531

Tian, H., Melillo, J. M., Kicklighter, D. W., McGuire, A. D., Helfrich, J. V., Moore, B., & VoÈroÈsmarty, C. J. (1998). Effect of interannual climate variability on carbon storage in Amazonian ecosystems. *Nature*, *396*(6712), 664–667. https://doi.org/10.1038/25328

Webb, J. R., Santos, I. R., Maher, D. T., Tait, D. R., Cyronak, T., & Jeffrey, L. C. (2018). Groundwater as a source of dissolved organic matter to coastal waters: Insights from radon and CDOM observations in 12 shallow coastal systems. *Limnology and Oceanography*, *64*(1), 182–196. https://doi.org/10.1002/lno.11028

Wilson, H. F., & Xenopoulos, M. A. (2009). Effects of agricultural land use on the composition of fluvial dissolved organic matter. *Nature Geoscience*, *2*(1), 37–41. https://doi.org/10.1038/ngeo391

Wymore, A. S., Potter, J., Rodríguez-Cardona, B., & McDowell, W. H. (2018). Using in situ optical sensors to understand the biogeochemistry of dissolved organic matter across a stream network. *Water Resources Research*, *54*, 2949–2958. https://doi.org/10.1002/2017WR022168

Yamashita, Y., & Tanoue, E. (2008). Production of bio-refractory fluorescent dissolved organic matter in the ocean interior. *Nature Geoscience*, *1*(9), 579–582. https://doi.org/10.1038/ngeo279

Yang, L., Guo, W., Chen, N., Hong, H., Huang, J., Xu, J., & Huang, S. (2013). Influence of a summer storm event on the flux and composition of dissolved organic matter in a subtropical river, China. *Applied Geochemistry*, *28*, 164–171. https://doi.org/10.1016/j.apgeochem.2012.10.004

Yang, L., Hong, H., Guo, W., Huang, J., Li, Q., & Yu, X. (2012). Effects of changing land use on dissolved organic matter in a subtropical river watershed, southeast China. *Regional Environmental Change*, *12*(1), 145–151. https://doi.org/10.1007/s10113-011-0250-9

Yang, L., Cheng, Q., Zhuang, W., Wang, H., & Chen, W. (2019). Seasonal changes in the chemical composition and reactivity of dissolved organic matter at the land-ocean interface of a subtropical river. *Environmental Science & Pollution Research*, *26*(24), 24,595–24,608. https://doi.org/10.1007/s11356-019-05700-2

Yoon, B., & Raymond, P. A. (2012). Dissolved organic matter export from a forested watershed during hurricane Irene. *Geophysical Research Letters*, *39*, L18402. https://doi.org/10.1029/2012GL052785

Yu, D., Yan, W., Chen, N., Peng, B., Hong, H., & Zhuo, G. (2015). Modeling increased riverine nitrogen export: Source tracking and integrated watershed-coast management. *Marine Pollution Bulletin*, *101*(2), 642–652. https://doi.org/10.1016/j.marpolbul.2015.10.035

Yuan, Y., & Yang, S. (2012). Impacts of different types of El Niño on the East Asian climate: Focus on ENSO cycles. *Journal of Climate*, *25*(21), 7702–7722. https://doi.org/10.1175/JCLI-D-11-00576.1

Zheng, Q., Fang, G., & Song, Y. (2006). Introduction to special section: Dynamics and circulation of the Yellow, East, and South China Seas. *Journal of Geophysical Research*, *111*, C11S01. https://doi.org/10.1029/2005JC003261